Eur. Phys. J. A (2013) **49**: 34
DOI 10.1140/epja/i2013-13034-7

THE EUROPEAN PHYSICAL JOURNAL A

Regular Article – Experimental Physics

Deep sub-threshold $K^*(892)^0$ production in collisions of Ar + KCl at 1.76 A GeV

The HADES Collaboration

G. Agakishiev[8], A. Balanda[3,†], R. Bassini[9], D. Belver[15], A.V. Belyaev[6], A. Blanco[2], M. Böhmer[11], J.L. Boyard[13], P. Cabanelas[15], E. Castro[15], S. Chernenko[6], T. Christ[11], M. Destefanis[8], J. Díaz[16], F. Dohrmann[5], A. Dybczak[3], T. Eberl[11], E. Epple[11], L. Fabbietti[11,a], O.V. Fateev[6], P. Finocchiaro[1], P. Fonte[2,b], J. Friese[11], I. Fröhlich[7], T. Galatyuk[7], J.A. Garzón[15], R. Gernhäuser[11], A. Gil[16], C. Gilardi[8], M. Golubeva[10], D. González-Díaz[4], F. Guber[10], M. Gumberidze[13], M. Heilmann[7], T. Heinz[4], T. Hennino[13], R. Holzmann[4], P. Huck[11], I. Iori[9,c,†], A. Ivashkin[10], M. Jurkovic[11], B. Kämpfer[5,d], K. Kanaki[5], T. Karavicheva[10], D. Kirschner[8], I. Koenig[4], W. Koenig[4], B.W. Kolb[4], R. Kotte[5,e], F. Krizek[14], R. Krücken[11], W. Kühn[8], A. Kugler[14], A. Kurepin[10], S. Lang[4], J.S. Lange[8], K. Lapidus[10,a], T. Liu[13], L. Lopes[2], M. Lorenz[7], L. Maier[11], A. Mangiarotti[2], J. Markert[7], V. Metag[8], B. Michalska[3], J. Michel[7], D. Mishra[8], E. Morinière[13], J. Mousa[12], C. Müntz[7], L. Naumann[5], J. Otwinowski[3], Y.C. Pachmayer[7], M. Palka[4], Y. Parpottas[12], V. Pechenov[4], O. Pechenova[8], T. Pérez Cavalcanti[8], J. Pietraszko[4], W. Przygoda[3], B. Ramstein[13], A. Reshetin[10], M. Roy-Stephan[13], A. Rustamov[4], A. Sadovsky[10], B. Sailer[11], P. Salabura[3], A. Schmah[11,f], E. Schwab[4], J. Siebenson[11], Yu.G. Sobolev[14], S. Spataro[8,g], B. Spruck[8], H. Ströbele[7], J. Stroth[7,4], C. Sturm[4], A. Tarantola[7], K. Teilab[7], P. Tlusty[14], M. Traxler[4], R. Trebacz[3], H. Tsertos[12], V. Wagner[14], M. Weber[11], C. Wendisch[5,d], M. Wisniowski[3], T. Wojcik[3], J. Wüstenfeld[5], S. Yurevich[4], Y.V. Zanevsky[6], and P. Zumbruch[4]

[1] Instituto Nazionale di Fisica Nucleare - Laboratori Nazionali del Sud, 95125 Catania, Italy
[2] LIP-Laboratório de Instrumentação e Física Experimental de Partículas, 3004-516 Coimbra, Portugal
[3] Smoluchowski Institute of Physics, Jagiellonian University of Cracow, 30-059 Kraków, Poland
[4] GSI Helmholtzzentrum für Schwerionenforschung GmbH, 64291 Darmstadt, Germany
[5] Institut für Strahlenphysik, Helmholtz-Zentrum Dresden-Rossendorf, 01314 Dresden, Germany
[6] Joint Institute of Nuclear Research, 141980 Dubna, Russia
[7] Institut für Kernphysik, Johann Wolfgang Goethe-Universität, 60438 Frankfurt, Germany
[8] II.Physikalisches Institut, Justus Liebig Universität Giessen, 35392 Giessen, Germany
[9] Istituto Nazionale di Fisica Nucleare, Sezione di Milano, 20133 Milano, Italy
[10] Institute for Nuclear Research, Russian Academy of Science, 117312 Moscow, Russia
[11] Physik Department E12, Technische Universität München, 85748 München, Germany
[12] Department of Physics, University of Cyprus, 1678 Nicosia, Cyprus
[13] Institut de Physique Nucléaire (UMR 8608), CNRS/IN2P3 - Université Paris Sud, F-91406 Orsay Cedex, France
[14] Nuclear Physics Institute, Academy of Sciences of Czech Republic, 25068 Rez, Czech Republic
[15] Departamento de Física de Partículas, Univ. de Santiago de Compostela, 15706 Santiago de Compostela, Spain
[16] Instituto de Física Corpuscular, Universidad de Valencia-CSIC, 46971 Valencia, Spain

Received: 10 December 2012 / Revised: 4 February 2013
Published online: 15 March 2013

Communicated by J. Äystö

Abstract. Results on the deep sub-threshold production of the short-lived hadronic resonance $K^*(892)^0$ are reported for collisions of Ar + KCl at 1.76 A GeV beam energy, studied with the High Acceptance Di-Electron Spectrometer (HADES) at SIS18/GSI. The $K^*(892)^0$ production probability per central collision of $P_{K^{*0}} = (4.4 \pm 1.1 \pm 0.5) \times 10^{-4}$ and the $K^*(892)^0/K^0$ ratio of $P_{K^{*0}}/P_{K^0} = (1.9 \pm 0.5 \pm 0.3) \times 10^{-2}$ are determined at the lowest energy so far (*i.e.* deep below the threshold for the corresponding production in nucleon-nucleon collisions, $\sqrt{s_{NN}} - \sqrt{s_{thr}} = -340$ MeV). The K^{*0}/K^0 ratio is compared with results of other experiments and with the predictions of the UrQMD transport approach and of the statistical hadronization model. The experimental K^{*0} yield and the K^{*0}/K^0 ratio are overestimated by the transport model by factors of about five and two, respectively. In a chemically equilibrated medium the ratio corresponds to a temperature of the thermalized system being systematically lower than the value determined by the yields of the stable and long-lived hadrons produced in Ar + KCl collisions. From the present measurement, we conclude that sub-threshold K^* production either cannot be considered to proceed in a system being in thermal equilibrium or these short-lived resonances appear undersaturated, for example as a result of the rescattering of the decay particles in the ambient hadronic medium.

1 Introduction

The short-lived resonance $K^*(892)^0$ (mass $M = 896\,\mathrm{MeV}$, decay width $\Gamma = 50\,\mathrm{MeV}$ corresponding to a mean lifetime $\tau = 4\,\mathrm{fm}/c$ [1]) can serve as a tool to study properties of the dense and hot nuclear matter produced in heavy-ion collisions. For instance, it has been conjectured [2] that the K^* yields reconstructed from hadronic decay products are sensitive to the thermal history of the fireball. Moreover, the phenomenologically successful thermo-statistical model [3–6] describes hadron yields over a large range of beam energies with system size and centrality effects partially included. It is interesting to consider also hadron excitations and ask whether they fit into the model. The neutral K^* is a vector excitation of the K^0 with valence quark structure $d\bar{s}$; K^{*0} suffers a p wave decay into $K^+\pi^-$ with a branching of 2/3 which is often used for its identification. Despite of the same quark structure, the $K^*(892)^+$ is predicted to obey a medium modification being quite different from that of K^+ [7]; a similar distinction might be expected for K^{*0} and K^0: While the K^0 is related to a repulsive potential in nuclear matter [8], the K^{*0} would be slightly attractive, provided it behaves similar to K^{*+}. These potentials are argued since a long time to influence the abundances of the respective hadrons (cf. [9] for a comprehensive discussion of such effects for $K^\pm$). Experimental data on K^* production in heavy-ion collisions are scarce and exist only since a few years. (For a review on strange hadron production in heavy-ion collisions from SPS to RHIC see [10].)

First LHC results on $K^*(892)^0$ production in pp collisions at $\sqrt{s_{NN}} = 7\,\mathrm{TeV}$ have recently been reported by the ALICE Collaboration [11]. While the K^* yield increases by about a factor of two from 200 GeV center-of-mass energy, the ratios ϕ/K^* and K^*/K are found to be independent of energy up to 7 TeV.

At RHIC energies, the STAR Collaboration reported on $K^*(892)^{0,\pm}$ production in Au + Au, Cu + Cu, and p+p collisions at $\sqrt{s_{NN}} = 62.4\,\mathrm{GeV}$ and 200 GeV [12,13]. The K^*/K yield ratios for all centralities and both energies in Au + Au and Cu + Cu collisions were smaller than the ratio in p + p interactions, leading to a nuclear modification factor less than unity. This finding indicates the importance of hadronic interactions after chemical freeze-out. The authors concluded that, at RHIC energies, the rescattering of the K^* decay products is dominant over the K^* regeneration.

At CERN-SPS energies, the NA49 Collaboration studied the production of $K^*(892)^0$ and $\bar{K}^*(892)^0$ in central Pb + Pb, Si + Si, C + C, and inelastic p + p collisions at 158 A GeV [14]. A strong decrease of the ratios $K^*(892)^0/K^+$ and their anti-particles with increasing system size of the colliding nuclei is reported. It is concluded that these ratios are most sensitive to interactions of the short-lived $K^*(892)^0$ and its decay daughters with the produced dense nuclear matter. Though the UrQMD transport approach [15,16] includes rescattering of K^{*0} and its daughters in the hadronic medium, this model was not able to describe $K^*(892)^0$ production in central Pb + Pb collisions, *i.e.* the $K^*(892)^0$ yield is overestimated by a factor of two.

No data is available on $K^*(892)^0$ production at AGS energies.

Sub-threshold production of $K^*(892)^0$ mesons has been first reported by the FOPI Collaboration at SIS18/GSI, measured in Al + Al collisions at 1.9 A GeV [17]. A $K^*(892)^0/K^0$ yield ratio of 0.032 ± 0.013 is found, in fair agreement with the corresponding prediction of the UrQMD transport model of 0.024. From the collision history, it is concluded that $K^+\pi^-$ fusion is the dominant process in sub-threshold $K^*(892)^0$ production.

In this article we report on the investigation of deep sub-threshold $K^*(892)^0$ production in collisions of Ar + KCl at a beam kinetic energy of 1.76 A GeV. In sect. 2 we shortly describe the experiment. In sect. 3 we present the analysis of the decay $K^*(892)^0 \to K^+\pi^-$ and discuss sources of systematic errors. In sect. 4 we present the output of Monte Carlo simulations used to correct the measured data for detector acceptance and reconstruction efficiency. In sect. 5 we compare the $K^*(892)^0$ production probability and the yield ratio $K^*(892)^0/K^0$ to the findings of other experiments and to model calculations. Finally, we summarize our results in sect. 6.

2 The experiment

The experiment was performed with the **H**igh **A**cceptance **D**i-**E**lectron **S**pectrometer (HADES) at the Schwerionensynchrotron SIS18 at GSI, Darmstadt. HADES, although primarily designed to measure di-electrons [18], offers excellent hadron identification capabilities [8,19–22] allowing for a profound correlation analysis. A detailed description of the spectrometer is presented in ref. [23]. The present results are based on a data set which was previously analyzed with respect to $K^\pm$, ϕ [20], Ξ^- [21], $\pi^\pm$, K^0 [8], Λ [22], and e^+e^- [24]. In the following we summarize the main features of the apparatus.

[a] *Also at*: Excellence Cluster Universe, Technische Universität München, 85748 Garching, Germany.
[b] *Also at*: ISEC Coimbra, Coimbra, Portugal.
[c] *Also at*: Dipartimento di Fisica, Università di Milano, 20133 Milano, Italy.
[d] *Also at*: Technische Universität Dresden, 01062 Dresden, Germany.
[e] e-mail: kotte@hzdr.de
[f] *Also at*: Lawrence Berkeley National Laboratory, Berkeley California 94720, USA.
[g] *Also at*: Dipartimento di Fisica Generale and INFN, Università di Torino, 10125 Torino, Italy.
[†] Deceased.

HADES consists of a 6-coil toroidal magnet centered on the beam axis and six identical detection sections located between the coils and covering polar angles from 18° to 85°. The six sectors consisted of hadron blind Ring-Imaging Cherenkov (RICH) detectors (not used for the present investigation), four planes of Multi-wire Drift Chambers (MDCs) for track reconstruction (with two opposite MDCs in the outermost plane not installed during the present experiment), and two time-of-flight walls, TOFino (polar angles $18 < \theta < 44$ degrees) and TOF ($44 < \theta < 88$ degrees), supplemented at forward polar angles with Pre-Shower chambers. The TOF and TOFino+Pre-Shower detectors were combined into a Multiplicity and Electron Trigger Array (META). A reconstructed track in the spectrometer is composed of straight inner and outer track segments in the MDCs. The pointing vector of the outer track segment is used for matching with a META hit. Possible trajectories through pairs of inner and outer track segments are combined to track candidates. A Runge-Kutta algorithm allows to calculate the momentum of each track candidate making use of the track deflection in the magnetic field. The quality of the META-hit matching and the Runge-Kutta fitting (characterized by χ^2 values) is used to create a list of ordered track candidates. The track candidate with the lowest product of both χ^2 values is selected as the true track. Its components and associated track candidates are then deleted from the candidate list. This procedure is repeated until no track candidates are left in the list.

Particle identification of K^+ and π^- mesons is based on the correlation of their momenta and velocities. The particle velocity is determined by the time of flight between a diamond start detector in the beam and the hit on the META detectors, and by the reconstructed flight path. At forward polar angles, where the particle identification suffers from multiple detector hits and poorer TOF resolution, in addition the correlation of momentum and energy loss of the particle in the MDCs is taken into account. Graphical cuts in the corresponding correlation plots are used to select the different particle species. Finally we note that, with the detector configuration of the present experiment, K^+ identification with a good signal-to-background ratio suited for correlation studies (*i.e.* signal/bg $\gg 1$) was possible only in four sectors of the TOF system. (Two opposite sectors were not yet produced for the outermost tracking plane.) Hence, we can analyze K^+ data from that phase-space region only, while π^- data are available from the full detector acceptance. For more details, *e.g.*, the quality of the K^+ identification, see refs. [19, 20].

A ^{40}Ar beam of about 10^6 nuclei per second with kinetic energy of 1.76 A GeV was incident on a four-fold segmented target of natural KCl with a segment interval of 8 mm and a total thickness of 5 mm corresponding to 3.3% interaction length. The position resolution (sigma) of the reaction vertex amounts to 0.3 mm in both transverse directions while in beam direction it amounts to 1.5 mm. The data readout was started by a first-level trigger (LVL1) decision, requiring a charged-particle multiplicity ≥ 16 in the TOF/TOFino detectors. The integrated cross section selected by this trigger comprises approximately the most central 35% of the total reaction cross section. The average value and the r.m.s. width of the corresponding impact parameter distribution following from UrQMD model calculations amount to 3.5 and 1.5 fm, respectively. Also, the mean number of participating nucleons in the LVL1-triggered reactions, $A_{part} = 38.5 \pm 2.7$, is estimated from UrQMD simulations [25, 26]. About $N_{ev} = 7.0 \times 10^8$ LVL1 events were processed for the present investigation.

3 Analysis of experimental data

Taking this high-statistics K^+ sample, we start the K^{*0} search by combining —for each event containing a K^+ candidate— the K^+ with all π^- mesons per event. The result is a structure-less K^+-π^- invariant-mass distribution. Hence, additional cuts were necessary. These are the one-particle conditions

- maximum values of the quality parameters of the inner and outer track segments, $\chi^2_{i,o}/\mathrm{ndf} < 25$, for both, K^+ and π^-,
- a maximum value of the Runge-Kutta track fitting quality parameter, $\chi^2_{RK}/\mathrm{ndf} < 30$, for both, K^+ and π^-,
- a maximum value of the quality of the matching distance of MDC tracks and META hits, $\chi^2_{META}/\mathrm{ndf} < 6$, for both, K^+ and π^-,
- a maximum value of the track distance to primary vertex, $d_{K^+,\pi^-} < 25$ mm for both, K^+ and π^-,
- a window of ± 65 MeV (± 120 MeV) around the nominal K^+ (π^-) mass,

and the two-particle conditions

- an upper limit of the distance of the pointing vector of the $K^+\pi^-$ pair w.r.t. the primary vertex, $d_p < 25$ mm,
- a maximum distance of the secondary K^{*0} vertex relative to the primary one, $d_v < 25$ mm,
- a maximum value of the distance of closest approach of the K^+ and π^- tracks, $d_t < 25$ mm,
- a minimum opening angle between K^+ and π^-, $\alpha_{K^+,\pi^-} > 30$ degrees, and
- limits to the momentum ratio of K^+ and π^-, $0.3 < |\boldsymbol{p}_{K^+}|/|\boldsymbol{p}_{\pi^-}| < 3.5$.

All cuts are applied for the generation of both, the intra-event and the inter-event (via event-mixing), invariant-mass distributions. About 300000 pairs fulfill the above conditions.

Figure 1 shows the resulting invariant-mass distribution. In the upper panel, the histogram displays the true yield derived from intra-event combinatorics. The dots show the scaled combinatorial background generated via event mixing. The shaded regions represent the area used for scaling the combinatorial background, *i.e.* the region of

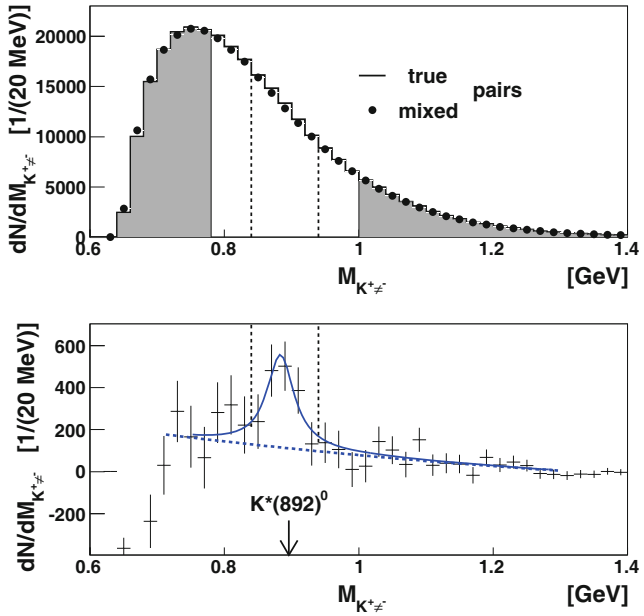

Fig. 1. Top: The invariant-mass distribution of $K^+\pi^-$ pairs in collisions of Ar + KCl at 1.76 A GeV. The histogram shows the true yield while the dots display the combinatorial background generated via event mixing. The shaded regions represent the area used for normalization. The vertical dashed lines mark the invariant-mass window (100 MeV) used for integration of the signal. Bottom: The invariant-mass distribution after subtraction of the combinatorial background (histogram with error bars). The full curve is a fit function consisting of a Breit-Wigner function (mean value $\langle M \rangle = (885 \pm 7)$ MeV, width $\Gamma = (48 \pm 21)$ MeV) and a polynomial of 2nd order used to account for a residual background. The dashed curve represents the polynomial. The arrow indicates the position of the $K^*(892)^0$ meson [1].

the expected K^{*0} peak is excluded from the normalization. The lower panel shows the resulting difference distribution. Similar to the observations at higher energies [12–14], there is some residual background, *i.e.* the invariant-mass distribution from event mixing does not properly describe the true background yield. Potential sources for that finding could be, *e.g.*, the energy-momentum conservation and the collective directed (side-) flow. Both effects can hardly be corrected in collision systems with small numbers of particles per event, as Ar + KCl. Furthermore, π^-p pairs from the decay of baryonic resonances (Δ, N^*), with the protons being misidentified as K^+ mesons, may contribute to a slight admixture of correlated background. Hence, the residual background is parameterized by a polynomial of 2nd order (dashed curve in lower panel) and fit together with the peak, which is either parameterized by a Breit-Wigner or a Gaussian distribution. The vertical lines bound the mass window around the expected peak position, 840 MeV $< M_{K^+\pi^-} <$ 940 MeV, used for integrating the signal yield. We performed extensive studies of the present invariant-mass distribution w.r.t. the stability of the rather weak signal. Finally, when averaging over the variation of i) the various cut parameters, ii) the normalization region, iii) the type of the peak-fit function, iv) the mass range of the fit, and v) the bin size of the histogram, we derive a $K^*(892)^0$ yield of

$$N_{K^{*0}} = 1070 \pm 262 \pm 93, \quad (1)$$

with the statistical error corresponding to an average significance of 4.1 and a systematic error following from the above variations. The signal-to-background ratio amounts to 0.017. Note that, to a large extent due to the restricted K^+ acceptance, the K^{*0} signal is mainly populated by slow $K^+\pi^-$ pairs. The distribution in rapidity of the K^{*0} signal relative to the center-of-mass value of 0.86 has a maximum around −0.4 and extends from −0.7 to −0.1.

4 Analysis of simulation data

Corrections for the finite acceptances and reconstruction efficiencies were deduced from simulations. Typically, one million thermal $K^*(892)^0$'s were generated with the fireball option (temperature of 90 MeV) of the event generator Pluto [27]. The choice of the temperature parameter follows from systematics of central heavy ion collisions in the 1 A GeV regime [28] and from the kinetic temperatures derived from the spectra of various hadrons carrying strangeness of comparable masses which are produced in Ar + KCl collisions at 1.76 A GeV [20, 22]. *A priori*, neither a certain deviation of the spectral shape parameter from this value nor some anisotropy in the phase-space distribution of the K^{*0} mesons can be excluded. Therefore, we allowed for a reasonable span of the temperature of ±20 MeV and a finite asymmetry parameter, $a_2 = [0, 1]$, in the center-of-mass polar-angle distribution, $dN/d\Theta_{cm} \propto 1 + a_2 \cos(\Theta_{cm})$, in accordance with the findings of the KaoS Collaboration for K^+ mesons [29]. The $K^*(892)^0$ are forced to decay into a single channel, $K^*(892)^0 \rightarrow K^+\pi^-$. The decay products, K^+ and π^-, were processed through GEANT [30], modeling the detector response. The GEANT data were then embedded (1/event) into real experimental data and processed through the full analysis chain. Relating the outputs, after cuts, to the corresponding inputs, the average K^{*0} acceptance and reconstruction efficiency was estimated to

$$\epsilon = (3.50 \pm 0.07 \pm 0.25) \times 10^{-3}. \quad (2)$$

(This value includes the branching ratio of 2/3 for the decay $K^{*0} \rightarrow K^+\pi^-$.) The statistical error in (2) reflects the K^{*0} yield left after the whole analysis of the simulation data, while the systematic error follows from the variation of the fireball temperature and the polar asymmetry in Pluto, similar to our previous studies of deep sub-threshold Ξ^- production [21]. It is worth to be mentioned that the UrQMD transport model simulation of the present collision system (see sect. 5) yields a slightly elongated momentum-space distribution. The geometrical acceptance derived from a Pluto run which reproduces the results of Maxwell-Boltzmann fits to the UrQMD distribution, *i.e.* the transverse ($T_\perp = (106 \pm 5)$ MeV) and

longitudinal shape parameters ($T_{\parallel} = (146 \pm 5)$ MeV; non-relativistic approximation from Gaussian rapidity width: $T_{\parallel} \approx M_{\mathrm{K}^*}\sigma_y^2 = (132 \pm 3)$ MeV), deviates by less than 1% from the value resulting from the reference parameters given above. Finally, we note that the apparatus mass resolution causes a K^{*0} width of 6.5 MeV when using a constant mass for the K^{*0} in the simulation.

5 Discussion

The $\mathrm{K}^*(892)^0$ production probability per LVL1 event amounts to

$$P_{\mathrm{K}^{*0}} = \frac{N_{\mathrm{K}^{*0}}}{\epsilon\, N_{ev}} = (4.4 \pm 1.1 \pm 0.5) \times 10^{-4}, \qquad (3)$$

where the statistical error follows from the statistical error of the $\mathrm{K}^*(892)^0$ signal (1) and the systematic error from both, the systematic error of the signal (cf. sect. 3) and the systematic error arising from the variation of the fireball parameters in the Pluto event generator. Taking into account the K^0 yield, $P_{\mathrm{K}^0} = 2P_{\mathrm{K}^0_S} = (2.3{\pm}0.1{\pm}0.18){\times}10^{-2}$, measured in the same experiment [8], the $\mathrm{K}^{*0}/\mathrm{K}^0$ yield ratio can be determined,

$$P_{\mathrm{K}^{*0}}/P_{\mathrm{K}^0} = (1.9 \pm 0.5 \pm 0.3) \times 10^{-2}. \qquad (4)$$

Now, we try to compare the present K^{*0} yield and $\mathrm{K}^{*0}/\mathrm{K}^0$ ratio to different experimental data, starting from maximum SIS18 energies up to LHC energies. Only few data are available concerning K^* production in heavy-ion collisions. For Al + Al collisions at 1.9 A GeV, the FOPI Collaboration reported a $\mathrm{K}^{*0}/\mathrm{K}^0$ ratio of 0.0315 ± 0.006(stat.) $\pm$ 0.012(syst.) and a K^0 yield of 0.038 ± 0.001(stat.) $\pm$ 0.004(syst.) [17]. The resulting K^{*0} yield is shown in fig. 2, together with our yield (3) and K^{*0} yields measured at maximum SPS [14], at RHIC [12,13], and at LHC energies [11]. Taking into account a steep decline of the excitation function for K^* production near and below threshold and considering the stronger centrality selection by FOPI (20% of the total geometrical cross section), our ratio (4) is in line with that value. No data are available in the intermediate region of the former AGS and at lower SPS energies, where the yield increases over three orders of magnitude. Here, the planned experiments at the future accelerator facilities FAIR in Darmstadt and NICA in Dubna may contribute significantly to the data base. All the other available data, from SPS to LHC, deliver quite similar K^{*0} yields per participant. The full curve in fig. 2 is a fit to all K^{*0} data with a function $f(x) = C(1-(D/x)^{\mu})^{\nu}$ ($x = \sqrt{s_{NN}}$, $C = 0.10$, $D = 2.54$ GeV, $\mu = 0.60$, $\nu = 2.1$), a simple parametrization which may be used to estimate the expected K^{*0} yield in energy regions, where data are not yet available. The smooth dashed curve connects data points (full dots) of the excitation function of K^+ production (taken from [9,31] and references cited therein) which is well reproduced by HSD [32] and UrQMD [15,16] transport model calculations. For better comparison with the K^{*0} data, the energy is shifted by the difference of the K^* and K^+ thresholds, $\sqrt{s_{thr,\mathrm{K}^*}} - \sqrt{s_{thr,\mathrm{K}^+}} = 0.4$ GeV, which refer to pp collisions. Obviously, the K^* and K excitation functions exhibit a very similar threshold behavior. Finally, we notice that in the SPS, RHIC, and LHC energy regions, the K^*/K ratio is more than an order of magnitude larger than our value (4), a result of the much higher energy density (respectively, a temperature approximating an upper limit of about 160 MeV) reached in heavy-ion collisions at these energies. However, the ratios do not vary much, except for central collisions of the largest systems (Pb + Pb, Au + Au), where a reduction of the K^*/K ratio is observed, indicating some influence of the ambient nuclear medium onto the short-lived K^* mesons and/or their decay daughters.

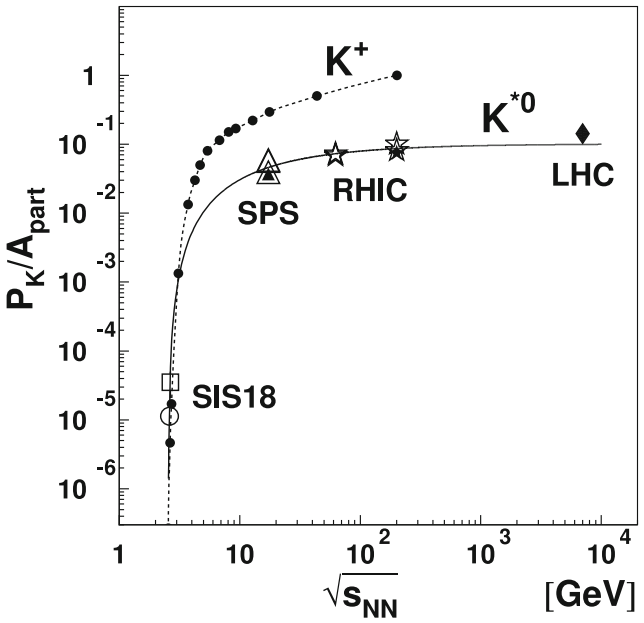

Fig. 2. The $\mathrm{K}^*(892)^0$ yield normalized to the number of participants as a function of $\sqrt{s_{NN}}$. The circle represents the HADES value (3) for Ar + KCl collisions. The square exhibits the K^{*0} yield for Al + Al collisions measured by FOPI at SIS18 [17]. Triangles show the K^{*0} data taken by NA49 at SPS [14] for p+p, C + C, Si + Si, and Pb + Pb collisions. The stars are the K^{*0} mid-rapidity yields $\mathrm{d}N/\mathrm{d}y$ ($|y| < 0.5$) measured by STAR at RHIC for p + p, Cu + Cu, and Au + Au collisions [12, 13], converted to total yields using the Gaussian rapidity width from NA49 [14]. Diamonds: The same for the K^{*0} mid-rapidity yield by ALICE at LHC [11]. Full triangles, stars and diamonds are for inelastic p+p reactions. The full curve is a parameterization to the data (see text). The dashed curve connecting the full dots represents the K^+ excitation function [9,31] shifted to the right by the difference of the K^* and K^+ thresholds of 0.4 GeV.

Next, we compare our results with model predictions. First, we start with the UrQMD transport approach [15, 16]. Reactions of Ar + KCl at 1.76 A GeV are simulated with an impact parameter distribution according to the experimental trigger of the most central 35% of the cross section, *i.e.* applying an impact parameter distribution $\mathrm{d}N/\mathrm{d}b \propto b$ with a maximum impact parameter of $b_{max} = 5.1$ fm. About 10^6 events have been processed.

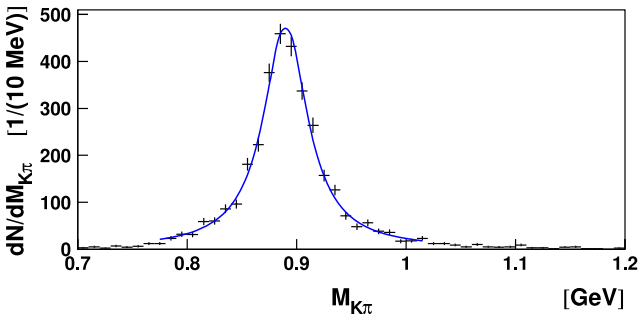

Fig. 3. The invariant-mass distribution of Kπ pairs from K* decays in collisions of Ar + KCl at 1.76 A GeV simulated with the UrQMD transport model. The full curve is a fit with a Breit-Wigner function (mean value: $\langle M \rangle = (890 \pm 1)$ MeV, width: $\Gamma = (49 \pm 1)$ MeV).

The resulting Kπ invariant-mass distribution is displayed in fig. 3. It exhibits a Breit-Wigner shaped peak with the mean value and the width being in accordance with the PDG values [1]. Here, the ideal particle identification from the model is used. Since only true Kπ pairs from K* decays contribute to the distribution, there is no background due to uncorrelated Kπ pairs or due to misidentification, in contrast to fig. 1. The K^{*0} yield per trigger event amounts to $(21.3 \pm 0.5) \times 10^{-3}$. It significantly overestimates (by a factor of 4.8) the experimental production probability (3), even more than observed by the NA49 Collaboration for central Pb + Pb collisions at SPS energies [14]. Furthermore, also the K^0 yield of 4.6×10^{-2} delivered by UrQMD is a factor of two larger than the corresponding experimental value [8]. Taking both numbers into account, we deduce a K^{*0}/K^0 ratio of 0.046 ± 0.001 which is overestimating the experimental ratio (4) by a factor of 2.4. Here we want to note, that a better reproduction of the absolute kaon yields might be achieved with transport models which include a repulsive kaon-nucleon potential. However, such an option to simulate the interaction with the nuclear medium is not available within UrQMD.

Another model comparison was performed with the statistical hadronization model. Within the Boltzmann approximation of this model, the freeze-out temperature is determined by the yield ratio of two mesons with identical strangeness and isospin,

$$T_{12} = (m_1 - m_2) \,/\, \ln \left[\left(\frac{2J_1 + 1}{2J_2 + 1} \right) \left(\frac{m_1}{m_2} \right)^{\frac{3}{2}} \left(\frac{P_2}{P_1} \right) \right], \quad (5)$$

where $m_{1,2}$ are the masses, $J_{1,2}$ the spins, and $P_{1,2}$ the production probabilities [4]. Inserting the corresponding values of K^{*0} and K^0 for particle species 1 and 2, respectively, we derive a temperature of

$$T_{\mathrm{K}^{*0}\mathrm{K}^0} = (67^{+3}_{-4}) \text{ MeV}. \quad (6)$$

The quoted error corresponds to the quadratic sum of the statistical and systematic errors of the involved yields. The temperature value (6) is in fair agreement with systematics of chemical freeze-out temperatures, derived (together with baryo-chemical potentials, μ_b) from thermal-model fits to particle ratios in central nucleus-nucleus collisions over a broad energy range. At an energy of $\sqrt{s_{NN}} = 2.7$ GeV, this fit yields a temperature of $T(\mathrm{Au} + \mathrm{Au}) = (64 \pm 1)$ MeV ($\mu_b = (760 \pm 20)$ MeV) [5]. However, the deduced temperature (6) differs from the result of a similar fit, applied to the yields of most of the stable hadrons and comparably long-lived resonances produced in collisions of the system Ar + KCl at an energy of 1.76 A GeV. Using the thermo-statistical model code THERMUS [6], one derives $T(\mathrm{Ar} + \mathrm{KCl}) = (76 \pm 2)$ MeV ($\mu_b = (799 \pm 22)$ MeV) [22]. Otherwise, when inserting $T(\mathrm{Ar} + \mathrm{KCl})$ into eq. (5), a K^{*0}/K^0 yield ratio of $(3.8^{+0.6}_{-0.5}) \times 10^{-2}$ would follow, significantly larger than the experimental value (4). The observation, that a reproduction of the yields (ratios) requires an apparently larger freeze-out temperature for smaller systems [22], has already been reported in ref. [3], indicating a more elaborated system-size dependence of the freeze-out border beyond a universal curve $f(T, \mu_b)$.

6 Summary

The data, for collisions of Ar + KCl at 1.76 A GeV beam energy, studied with the High Acceptance Di-Electron Spectrometer (HADES) at SIS18/GSI, exhibit a clear K$^*(892)^0$ signal. This allows for the determination of the K^{*0} yield per central event (defined by selecting the most central 35% of the total cross section) of $(4.4 \pm 1.1 \pm 0.5) \times 10^{-4}$ in heavy-ion collisions at the lowest energy so far, *i.e.* deep below the threshold for the corresponding production in nucleon-nucleon collisions, $\sqrt{s_{NN}} - \sqrt{s_{thr}} = -340$ MeV. We observe a quite similar threshold behavior of the K^{*0} yield as for K$^+$ production.

Applying the UrQMD transport approach, we found that the experimental K^{*0} production yield and the K^{*0}/K^0 ratio are overestimated by factors of 4.8 and 2.4, respectively. Less discrepancies might appear if in-medium modifications of kaon properties could be incorporated into this transport model.

Using the statistical hadronization model, the deduced K^{*0}/K^0 ratio allows to calculate the freeze-out temperature which is in agreement with systematics generated with the thermo-statistical model for central Au + Au/Pb + Pb collisions. However, the resulting temperature is smaller than the value derived from a global statistical-model fit to the yields of the majority of the particles produced in Ar + KCl collisions. This observation may lead to different interpretations. Either subthreshold K$^*(892)^0$ production cannot be considered to proceed in a system being in thermal equilibrium. Or, more probably, our findings hint to an undersaturation of these short-lived resonances of about 50%, primarily due to rescattering of the decay particles in the ambient hadronic medium, resulting in the dispersion of part of the resonant K^{*0} yield in the uncorrelated K$^+\pi^-$ background. Finally, the suspicion that K^{*0} freeze-out occurs at a reduced temperature level is less conceivable.

The HADES Collaboration gratefully acknowledges the support by BMBF grants 06DR9059D, 06FY171, 06MT238 T5, and 06MT9156 TP5, by HGF VH-NG-330, by DFG EClust 153, by GSI TMKRUE, by the Hessian LOEWE initiative through HIC for FAIR (Germany), by grants MSMT LC07050 and GA ASCR IAA100480803 (Czech Rep.), by grant KBN 1P03B 056 26 (Poland), by grants FPA2006-09154 and CPAN:CSD2007-00042 (Spain), by grant UCY-10.3.11.12 (Cyprus), by CNRS/IN2P3 (France), by INFN (Italy), and by EU contracts RII3-CT-2005-515876 and HP2 227431.

References

1. Particle Data Group (K. Nakamura *et al.*), J. Phys. G Nucl. Part. Phys. **37**, 075021 (2010).
2. G. Torrieri, J. Rafelski, Phys. Rev. C **75**, 024902 (2007).
3. F. Becattini, J. Manninen, M. Gazdzicki, Phys. Rev. C **73**, 044905 (2006).
4. J. Randrup, J. Cleymans, Phys. Rev. C **74**, 047901 (2006).
5. A. Andronic, P. Braun-Munzinger, J. Stachel, Nucl. Phys. A **772**, 167 (2006).
6. S. Wheaton, J. Cleymans, Comput. Phys. Commun. **180**, 84 (2009).
7. K. Tsushima, A. Sibirtsev, A.W. Thomas, Phys. Rev. C **62**, 064904 (2000).
8. HADES Collaboration (G. Agakishiev *et al.*), Phys. Rev. C **82**, 044907 (2010).
9. C. Hartnack, H. Oeschler, Y. Leifels, E.L. Bratkovskaya, J. Aichelin, Phys. Rep. **510**, 119 (2012).
10. C. Blume, C. Markert, Prog. Part. Nucl. Phys. **66**, 834 (2011).
11. ALICE Collaboration (B. Abelev *et al.*), Eur. Phys. J. C **72**, 2183 (2012).
12. STAR Collaboration (J. Adams *et al.*), Phys. Rev. C **71**, 064902 (2005).
13. STAR Collaboration (M.M. Aggarwal *et al.*), Phys. Rev. C **84**, 034909 (2011).
14. NA49 Collaboration (T. Anticic *et al.*), Phys. Rev. C **84**, 064909 (2011).
15. S.A. Bass *et al.*, Prog. Part. Nucl. Phys. **41**, 255 (1998).
16. M. Bleicher *et al.*, J. Phys. G **25**, 1859 (1999).
17. FOPI Collaboration (X. Lopez *et al.*), Phys. Rev. C **81**, 061902 (2010).
18. HADES Collaboration (G. Agakichiev *et al.*), Phys. Rev. Lett. **98**, 052302 (2007).
19. A. Schmah, PhD thesis, Techn. Universität Darmstadt (2008).
20. HADES Collaboration (G. Agakishiev *et al.*), Phys. Rev. C **80**, 025209 (2009).
21. HADES Collaboration (G. Agakishiev *et al.*), Phys. Rev. Lett. **103**, 132301 (2009).
22. HADES Collaboration (G. Agakishiev *et al.*), Eur. Phys. J. A **47**, 21 (2011).
23. HADES Collaboration (G. Agakichiev *et al.*), Eur. Phys. J. A **41**, 243 (2009).
24. HADES Collaboration (G. Agakishiev *et al.*), Phys. Rev. C **84**, 014902 (2011).
25. HADES Collaboration (P. Tlusty *et al.*), in *Proceedings of the XLVII International Winter Meeting on Nuclear Physics, Bormio, Italy, Jan 26-30, 2009*, arXiv:0906.2309 (2009).
26. HADES Collaboration (G. Agakishiev *et al.*), Eur. Phys. J. A **40**, 45 (2009).
27. I. Fröhlich *et al.*, Proc. Sci. **PoS(ACAT)**, 076 (2007).
28. FOPI Collaboration (W. Reisdorf *et al.*), Nucl. Phys. A **848**, 366 (2010).
29. KaoS Collaboration (A. Förster *et al.*), Phys. Rev. C **75**, 024906 (2007).
30. GEANT 3.21, `http://consult.cern.ch/writeup/geant/` (1993).
31. E.L. Bratkovskaya, M. Bleicher, M. Reiter, S. Soff, H. Stöcker, M. van Leeuwen, S.A. Bass, W. Cassing, Phys. Rev. C **69**, 054907 (2004).
32. W. Cassing, E.L. Bratkovskaya, S. Juchem, Nucl. Phys. A **674**, 249 (2000).